




Scaling the Diurnal Mixing/Mixed Layer Depth in the Tropical Ocean: A Case Study in the South China Sea

Zhiyong Cao^{1,2}, Zhiyu Liu¹ , Dong Wang¹ , Jianing Wang² , Hongyang Lin¹ , and Fangtao Zhang¹

¹State Key Laboratory of Marine Environmental Science, and Department of Physical Oceanography, College of Ocean and Earth Sciences, Xiamen University, Xiamen, China, ²Key Laboratory of Ocean Observation and Forecasting and Key Laboratory of Ocean Circulation and Waves, Institute of Oceanology, Chinese Academy of Sciences, Qingdao, China

Key Points:

- Diurnal cycling of stratification and turbulence is ubiquitous in the tropical upper ocean, even in winter
- A new scaling of the diurnal mixing/mixed layer depth in terms of sea surface variables (wind speed, air-sea heat flux, and sea surface temperature) is proposed and tested
- It provides a simple way to predict the diurnal mixing/mixed depth with solely surface observations

Correspondence to:

Z. Liu,
zylui@xmu.edu.cn

Citation:

Cao, Z., Liu, Z., Wang, D., Wang, J., Lin, H., & Zhang, F. (2024). Scaling the diurnal mixing/mixed layer depth in the tropical ocean: A case study in the South China Sea. *Journal of Geophysical Research: Oceans*, 129, e2024JC021296. <https://doi.org/10.1029/2024JC021296>

Received 3 MAY 2024

Accepted 8 SEP 2024

Author Contributions:

Conceptualization: Zhiyu Liu
Data curation: Fangtao Zhang
Formal analysis: Zhiyong Cao
Funding acquisition: Zhiyu Liu
Investigation: Zhiyong Cao
Methodology: Zhiyu Liu
Project administration: Zhiyu Liu
Supervision: Zhiyu Liu
Visualization: Zhiyong Cao
Writing – original draft: Zhiyong Cao
Writing – review & editing: Zhiyu Liu, Dong Wang, Jianing Wang, Hongyang Lin

Abstract The diurnal cycling of the surface mixing/mixed layer (ML) depth, air-sea heat flux, and vertical profiles of the temperature and turbulent kinetic energy dissipation rate in the tropical central South China Sea was observed in summer (June 2017) and winter (January 2018). In the daytime, solar heating warmed and stabilized the ML, and the thickness of the ML can be well characterized by the Zilitinkevich scale as noted in previous studies. By contrast, in the nighttime the ML was deepened by convective turbulence generated by surface cooling. Guided by these observations, we have derived a simple scaling for the nighttime deepening of the ML by simplifying the classic Kraus-Turner type model. We show that the variation of the ML depth can be scaled by a function of the wind speed, air-sea heat flux and the temporal variation of the sea surface temperature, all of which are observable variables at the sea surface. It is found that the scaling works well in reproducing observed variations of the ML depth from hydrographic data. As such, this study advances our understanding of the response of the upper ocean to atmospheric forcing and provides a simple way for predicting the ML depth with solely surface observations.

Plain Language Summary The mixed layer (ML) is the well-mixed region of the upper ocean, which is mainly influenced by air-sea interactions (e.g., wind forcing and buoyancy fluxes). The ML deepening/shoaling processes is critically important for physical, chemical, and biological oceanography. The diurnal variation of the ML depth is caused by daytime heating and nighttime cooling. In the daytime, the surface water gains heat (buoyancy), and then a shallow stable ML (with a thickness of several meters) is formed by the stirring of wind. In the nighttime, by contrast, the surface water loses heat (buoyancy) making the shallow ML unstable, and then the thickness of ML will develop to tens of meters. In this study, we propose a new method to estimate the diurnal variation of the ML depth with wind speed, air-sea heat flux, and sea surface temperature, all of which are observable variables at the sea surface. Our method well characterizes the observed ML depth throughout the diurnal cycle, making it possible to approximate the upper ocean structure without underwater data.

1. Introduction

The surface mixed layer (ML) is the near-surface layer of the ocean with a nearly uniform vertical density profile, which is a result of the vigorous mixing due to atmospheric forcing through wind, waves, and unstable buoyancy fluxes. As the intermediate layer between the atmosphere and the vast interior ocean, the ML controls atmosphere-ocean exchanges of the momentum, heat, and material tracers. Although the ML is only a thin layer (usually a few tens of meters at low and middle latitudes) of the upper ocean, it is an important component of the global climate system (Belcher et al., 2012). The ML depth (MLD) is a key factor for the upper ocean to absorb (and store) heat from the atmosphere owing to the high specific heat capacity of the water as compared to the air, and it is also closely related to the sea surface temperature (SST) on both the seasonal (Somavilla et al., 2017) and diurnal (Kawai & Wada, 2007; Zheng & Jing, 2024) timescales. However, the state-of-the-art climate models remain subject to large errors in predicting both the MLD and SST (Belcher et al., 2012; D'Asaro, 2014; C Huang et al., 2007). The deepening/shoaling processes of ML are mainly controlled by the wind stress, surface buoyancy flux, etc (Lozovatsky et al., 2005; Marshall & Schott, 1999; Somavilla et al., 2017). Therefore, a quantitative understanding of the variation of MLD and the scaling to the external forcing is crucially important.

The MLD is often discussed in terms of its seasonal variation (H denotes the seasonal mixed layer depth), but in the tropical ocean, it varies substantially during a diurnal cycle (h denotes the diurnal mixed layer depth)

(Brainerd & Gregg, 1993; Lombardo & Gregg, 1989; Shay & Gregg, 1984). Furthermore, the diurnal ML is composed of a diurnal warm layer (DWL) and a diurnal convective layer (DCL) which are formed by daytime heating and nighttime cooling, respectively. To discuss the diurnal variation of the ML, it is important to distinguish the mixed and mixing layer depth (MLD vs. XLD, denoted by h_ρ and h_ε , respectively).

The XLD is defined as the depth of the near-surface layer with vigorous mixing owing to surface forcing. Operationally, it can be determined as the depth where the turbulent kinetic energy (TKE) dissipation rate (denoted by ε) has decreased to an assumed background value independent of the surface forcing (Brainerd & Gregg, 1995; Franks, 2014; Sutherland et al., 2014). The dissipation rate represents the influence of different turbulence sources (i.e., wind stress and buoyancy loss), which is useful to the study of the dynamic process of the mixing layer. Recently, Giunta and Ward (2022) proposed a new method based on the shape of the dissipation profile for estimating h_ε (at which the ε values drop rapidly). By contrast, the MLD is defined according to the hydrological properties of the water column, which is usually calculated using a density threshold or temperature threshold relative to an operationally defined surface density or temperature, respectively (Boyer Montégut et al., 2004; Kara et al., 2000). There are also other definitions and estimations such as using a density gradient threshold (Lukas & Lindstrom, 1991) and the objective method (Chu & Fan, 2010; Holte & Talley, 2009; P Huang et al., 2018; Thomson & Fine, 2003). The common feature of these MLD definitions is to determine the thickness of the near-surface well-mixed water column by inspecting vertical profiles of the density or temperature. The XLD and MLD are dynamically related although they are not necessarily identical at any time. Physically, any mixed layer is developed from a mixing layer. The fundamental difference is that the mixed and mixing layers refer to different timescales over which mixing occurs. Besides physical distinctions between the XLD and MLD, thresholds used in operational calculations also contribute to the difference in their estimates (Sutherland et al., 2014). Both XLD and MLD actively respond to the diurnal external forcing and can be used to characterize the thickness of the DWL or DCL.

In the daytime, a DWL is formed due to the absorption of solar radiation. The thickness of the DWL can range from several centimeters to tens of meters which depends mainly on the wind speed (Soloviev & Lukas, 1997). Early studies suggest that the thickness of DWL is proportional to the Monin-Obukhov length ($L_{MO} = u_*^3 / (\kappa B_0)$), where $u_* = \sqrt{\tau / \rho_0}$ is the surface frictional velocity, τ is the surface wind stress, κ the von Kármán constant, and B_0 the surface buoyancy flux, expressing the relative roles of shear and buoyancy in the production of the TKE (Kraus & Turner, 1967). By incorporating the Ekman length scale ($\lambda = u_* f$), Zilitinkevich (1972) considered the effect of the Coriolis force and proposed the Zilitinkevich scale ($L_Z = \sqrt{L_{MO} \lambda}$). Recently, a few studies of large-eddy simulations (Goh & Noh, 2013; Noh & Choi, 2018; Ushijima & Yoshikawa, 2019; Yoshikawa, 2015) have confirmed that L_Z is more suitable for observed mixing/mixed layer depth than other length scales under stabilizing buoyancy flux, at least at low latitudes. Besides the scaling depth, Price et al. (1986) introduced two diagnostic depths (trapping depth D_T and penetration depth D_P) associated with restratification, the definitions of which are listed in Table 1.

In the nighttime, the previous warmer layer turns into the DCL as the surface water loses heat (buoyancy) which drives convective overturns. Using Thorpe overturning scale analysis, Brainerd and Gregg (1995) suggested that the Thorpe scale (L_T) could be a useful representation of the DCL depth. Shay and Gregg (1984) reported the first evidence that the TKE dissipation rate of the DCL is related to the lost buoyancy, $\varepsilon \sim B_0$. The deepening of the convective layer has been studied with laboratory experiments (Deardorff et al., 1969) and numerical simulations (Marshall & Schott, 1999). It has been suggested that the thickness of the convective layer increases according to

$$h_{MS} = \sqrt{\frac{2 \int B_0 dt}{N_{th}^2}}, \quad (1)$$

where N_{th} indicates density stratification in the thermocline just below the convective layer. However, Equation 1 does not seem to predict the observed deepening of the mixed layer well in winter, presumably because it ignores the contributions of the vertical mixing and advection (Somavilla et al., 2017).

The diurnal mixing/mixed layer depth is the consequence of the upper ocean's response to various external forcing, and thus the former should be represented as a function of the latter. In previous studies, the XLD/MLD was calculated based on the dissipation or density profiles, but continuous high-frequency (to reveal diurnal

Table 1
Diffident Depths of the Mixed Layer Used in This Study

Depth	Type	Definition	Description
h_e	I	ϵ background value: $1 \times 10^{-9} \text{ W kg}^{-1}$	Dissipation threshold (XLD)
h_ρ	I	$\Delta\rho = 0.03 \text{ kg m}^{-3}$ (in summer) $\Delta\rho = 0.01 \text{ kg m}^{-3}$ (in winter)	Density threshold (MLD)
h_N	I	Where N^2 is the maximum in the mixed layer	Stratification method
h_{ov}	I	Where S_ρ decreases to 0	The lower boundary of the first overturning
D_T	II	$D_T = \frac{1}{T'_s} \int_{z_r}^{z_s} T' dz$	The mean depth of the temperature anomaly
D_P	II	$D_P = \frac{Q_0}{\rho_0 c_p} \left(\frac{\partial T'_e}{\partial t} \right)^{-1}$	The depth scale in the one-dimensional heat equation
L_{MO}	III	$L_{MO} = u_*^3 / (\kappa B_0)$	The relative contribution of wind and buoyancy to TKE
L_Z	III	$L_Z = u_*^2 / (f B_0)^{\frac{1}{2}}$	The L_{MO} considered the geostrophic effect
h_{MS}	IV	$h_{MS} = \sqrt{\frac{2 \int B_0 dt}{N_h^2}}$	The deepening of the convective layer

Note. Type I indicates the observed depth. Type II indicates the diagnostic depth in stable stratification. Type III (IV) indicates the parameterized depth in stable (unstable) stratification.

variations) observations remain sparse. In this study, we seek to reveal the diurnal cycling of the XLD/MLD with field observations, aiming in particular at deriving a simple scaling for the evolution of XLD/MLD with solely surface observations. We will show that the variation of the XLD/MLD can be scaled by a functional combination of the wind speed, air-sea heat (buoyancy) flux, and the temporal variation of the SST, all of which are observable variables at the sea surface rather than the full depth profiles. This paper proceeds as follows. The data employed in our analysis are introduced in Section 2. The results are presented and discussed in Section 3. This paper concludes with a summary and discussion in Section 4.

2. Data and Methods

2.1. Observations

The data used in this study were obtained from a time series station in the central basin (116°E, 14°N; the red pentagram in Figure 1) of the South China Sea but in two different seasons. The summer cruise was performed on June 14–17, 2017 and the winter cruise was performed on January 25–26, 2018 (all time in this article is local time). Both of the two research cruises were conducted onboard the R/V TAN KAN KEE and in total 55 (18) vertical turbulence profiles and 53 (26) regular hydrographic profiles were collected in summer (winter). Besides, by using XCTD (eXpendable Conductivity-Temperature-Depth), we performed a rapid survey of two orthogonal transects after completing the time series observations in the summer cruise (Figure 1).

Turbulence microstructure measurements were made by using a free-fall vertical microstructure profiler (VMP, Rockland Scientific Inc.), which was equipped with two shear probes (sampled at 512 Hz), two FP07 fast-response thermistor and SBE3/4 temperature/conductivity sensors. The TKE dissipation rate ϵ was calculated by fitting the Nasmyth spectrum to the measured shear spectra over consecutive segments of 2 s (Roget et al., 2006; Volk et al., 2002). As a result, vertical profiles of ϵ have a resolution of ~ 1.2 m for the falling speed of the instrument of around 0.6 m/s. Due to contaminations by the ship's wake, the turbulence measurements and thus the estimated ϵ were unreliable in the upper 10 m of the water column; these data were therefore excluded from further analysis.

CTD (Conductivity-Temperature-Depth, SBE 911plus) casts were also conducted to obtain measurements of the temperature and salinity for comparison and the data have been averaged into 0.1 m bins. Measurements of the velocity were made using a 300 kHz ship-mounted acoustic Doppler current profiler (ADCP). Underway data collected during the two cruises include the near-surface (~ 5 m depth) temperature and salinity and meteorological data (e.g., wind speed, sea-surface air temperature, precipitation, relative humidity, solar radiation) were collected to provide observations of the atmospheric forcing. Surface fluxes are thus estimated using bulk formulae (Fairall et al., 2003) applied to standard ship meteorological measurements.

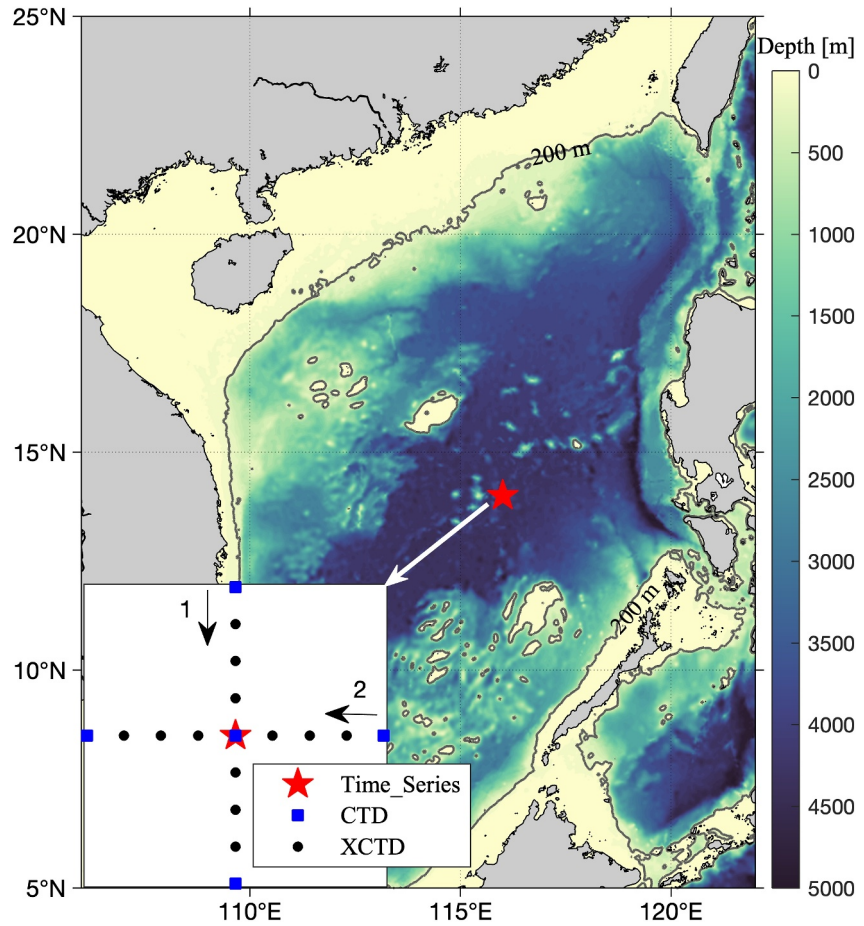


Figure 1. Topography of the South China Sea. Red pentagram marks the time series station and two orthogonal 18.5 km-long transects (inset, Sect. 1 and Sect. 2) were performed after time series survey in the summer cruise.

In general, the penetrative radiation of shortwave heat flux is given by the double-exponential model (Paulson & Simpson, 1977):

$$q(z) = (1 - albedo) Q_{sw} [R e^{-z/\gamma_1} + (1 - R) e^{-z/\gamma_2}], \quad (2)$$

where z is negative downward, $(1 - albedo) Q_{sw}$ is the downward shortwave radiation just below the sea surface and a constant $albedo = 0.06$ is adopted following Ohlmann and Siegel (2000), R , γ_1 , and γ_2 are constants depending on the water types (Paulson & Simpson, 1977). Besides the surface shortwave radiation, the net infrared long-wave radiation (Q_{lw}), latent heat flux (Q_l) due to evaporation, and sensible heat flux (Q_s) due to air-sea temperature difference also contribute to the net surface heat flux (Q_0):

$$Q_0 = (1 - albedo) Q_{sw} + Q_{lw} + Q_l + Q_s. \quad (3)$$

The fluxes are defined as downward positive, and thus positive fluxes indicate that the ocean gains heat and negative fluxes indicate that the ocean loses heat. The air-sea heat flux and freshwater flux (through evaporation E and precipitation P) combine to induce buoyancy flux at the air-sea interface, thus stabilizing or de-stabilizing the water column. The surface buoyancy flux can be quantified as:

$$B_0 = g\alpha Q_0 / \rho_0 c_p - g\beta s_0 (E - P), \quad (4)$$

where g , ρ_0 , c_p , and s_0 are the gravitational acceleration, a reference density of seawater, specific heat of water, and surface salinity, respectively, and α is the effective thermal expansion coefficient, β is the saline contraction coefficient.

2.2. Definitions of Depths

Depths in this study can be subdivided into four types and their definitions and descriptions are listed in Table 1. Type I means observed depth, including h_p , h_e , h_N , and h_{ov} . Here, h_p (h_e) is defined by the threshold method of density (dissipation) profiles; h_N is defined by the gradient method, and is chosen as the depth of maximum stratification in the mixed layer; h_{ov} is the lower boundary of the uppermost overturning of the density profile. To determine h_{ov} (Jalali et al., 2017): (a) Sort the density profile of the entire column into a stable monotonic profile; (b) Find vertical displacement (d_p) for each point between the sorted and unsorted profiles; (c) Calculate accumulation of displacements from the surface (S_p); (d) Determine the depth (h_{ov}) where S_p decreases to 0. Type II is the diagnostic depth including trapping depth D_T and penetration depth D_p , which was introduced by Price et al. (1986). They can determine the thickness of DWL with temperature profile and air-sea heat flux in stable stratification. Type III (IV) is the parameterized depth in stable (unstable) stratification. As a reference, we calculate the seasonal mixed layer depth (H), which is defined the same as h_p , but with the threshold $\Delta\rho = 0.3 \text{ kg m}^{-3}$.

3. Results

3.1. Atmospheric and Oceanic Background

The time series of the key meteorological and oceanic variables are shown in Figure 2. It was sunny in summer and cloudy in winter during the field observations. In the summer, the wind speed was low and ranged from 2.5 to 7.5 m s^{-1} , and the wind direction was around 225° (typical southwesterly monsoon). In the winter, in contrast, the wind was in the opposite direction (45°, typical northeasterly monsoon) and the wind was stronger and more fluctuating than summer. The wind speed for the duration of the deployment was low so the wave-breaking rate and wave-breaking intensity would therefore also be expected to be low. As characteristic of the subtropics, the sea-surface air temperature generally remained lower than SST even in winter, indicating negative sensible heat flux (Q_s) throughout the year. Both long-wave radiation (Q_{lw}) and latent heat flux (Q_l) were also negative throughout the year, causing heat loss from the surface ocean to the atmosphere. However, in the daytime large solar shortwave radiation (Q_{sw}) dominated the net surface heat flux inducing net heat gain of the surface ocean. The buoyancy flux was dominated by heat flux for there was no precipitation during the observation period. Consequently, the net surface heat (buoyancy) flux followed a typical diurnal cycle with surface cooling at night and heating during the day.

The mean profiles of the temperature (T), density (σ), buoyancy frequency (N^2), and TKE dissipation rate exhibited diurnal variations in the upper ocean both in summer and winter (Figure 3). The density ratio $R_\rho = \alpha(\partial T/\partial z)/\beta(\partial S/\partial z)$ was calculated (it denotes the relative contribution of the vertical gradient of temperature and salinity to the stratification, not shown), and the stratification was completely dominated by temperature in the summer cruise, except for the first day. In the winter cruise, by contrast, the contributions of temperature and salinity to stratification are equally important. The warm and light DWL was distinct in the upper ~10 m in daytime, especially in summer. Due to the different mechanisms of the DWL and the DCL, the stratification (dissipation) in daytime was 1–2 orders of magnitude larger (smaller) than that in nighttime within the upper mixed layer. In addition, the mean seasonal mixed layer depth (the horizontal black lines in Figure 3a) was 43 m in summer and 55 m in winter.

3.2. Diurnal Cycle of the ML

In order to highlight the diurnal signal, we calculate the vertical anomaly of temperature and density in the same manner as Price et al. (1986), that is,

$$T'(z, t) = T(z, t) - T(z_r, t), \quad (5)$$

$$\sigma'(z, t) = \sigma(z, t) - \sigma(z_r, t), \quad (6)$$

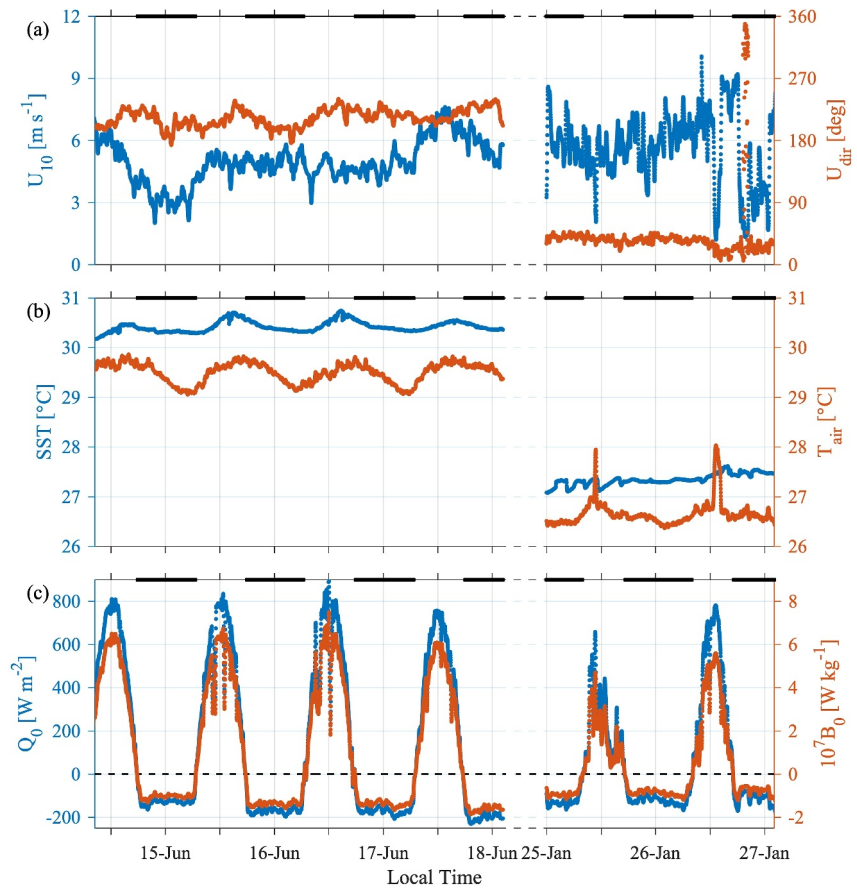


Figure 2. Time series of (a) 10 m wind speed U_{10} and direction U_{dir} (0° implies wind from the north), (b) SST and air temperature T_{air} , (c) net surface heat flux Q_0 and buoyancy flux B_0 . The black bar on the top axis indicates the time when Q_0 is negative (roughly represents the nighttime and the same for the following figures).

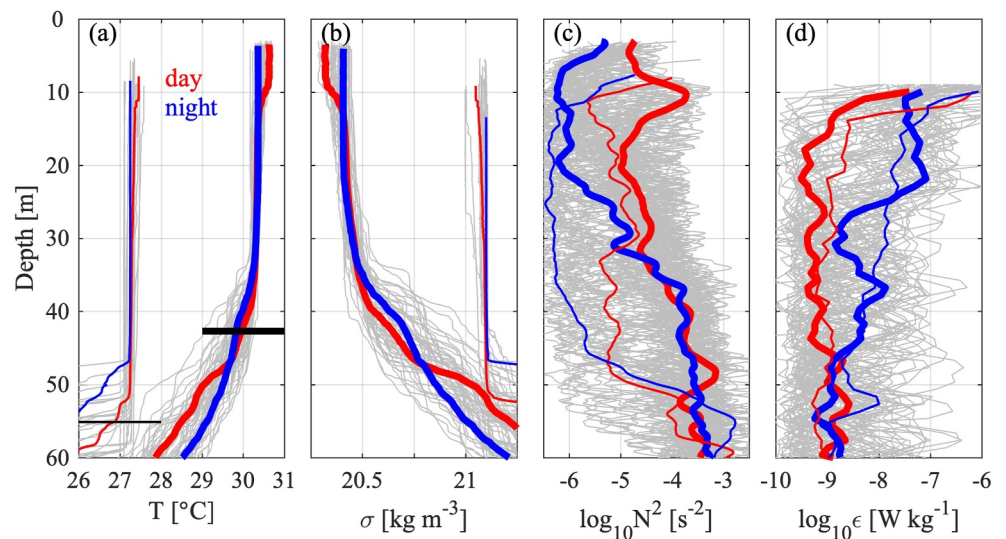


Figure 3. Daytime (red) and nighttime (blue) mean profiles of (a) temperature T , (b) density σ , (c) stratification N^2 and (d) dissipation rate ϵ . Bold (thinner) lines indicate the mean profiles in summer (winter). Horizontal black lines in panel (a) indicate the mean seasonal mixed layer depth (H).

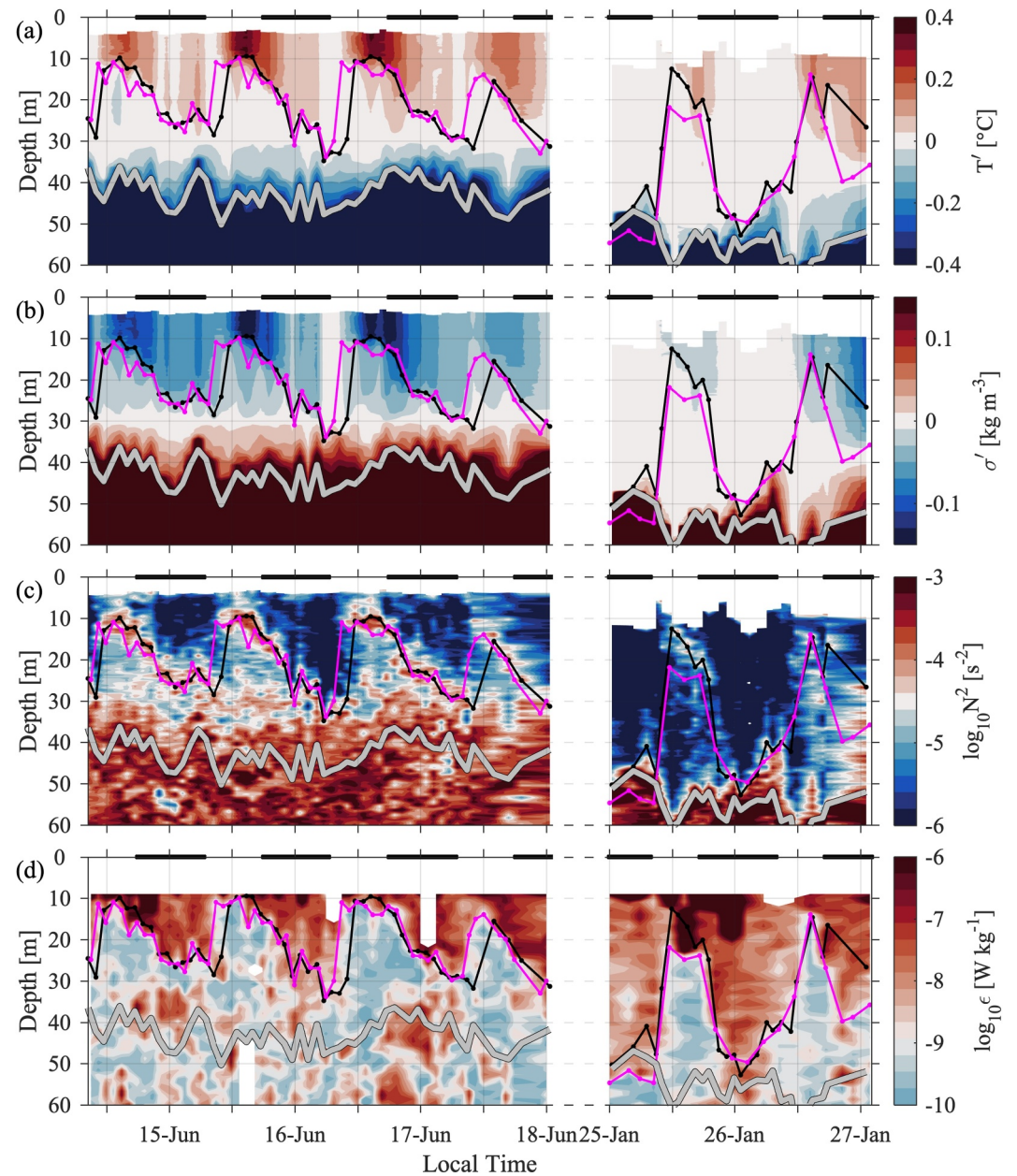


Figure 4. Time-depth evolution of (a) temperature anomaly T' , (b) density anomaly σ' , (c) stratification N^2 and (d) dissipation rate ϵ . The black, magenta, and gray lines denote h_ρ , h_e and H , respectively.

where z_r is the reference depth, which is chosen carefully to be deep enough to avoid the diurnal signal, and at the same time shallow enough to exclude the seasonal pycnocline. Reference depths of 30 m for summer and 45 m for winter are chosen according to the mean profiles shown in Figure 3. The time-depth evolutions of T' , σ' , N^2 , and ϵ are shown in Figure 4. All of them exhibit distinct diurnal cycling patterns, accompanied by a shallow DWL in the daytime and deepening DCL in the nighttime. The DWL and DCL can be clearly identified from h_ρ and h_e , where h_ρ is defined by the density threshold of 0.03 kg m^{-3} (0.01 kg m^{-3} in January) relative to the surface density (Boyer Montégut et al., 2004) and h_e is the depth where dissipation decreased to the assuming background level of $10^{-9} \text{ W kg}^{-1}$ (Sutherland et al., 2014). We have also tested the sensitivity of MLDs to different threshold values, and the variances of MLDs are generally minor. For instance, h_ρ varies from 26.5 to 29.4 m (Figure 5b) by adopting the density thresholds of 0.01 and 0.05 kg m^{-3} , respectively. In summer, the diurnal variation of temperature (density) was robust and up to 0.4°C (0.15 kg m^{-3}), while in winter it became much weaker. These

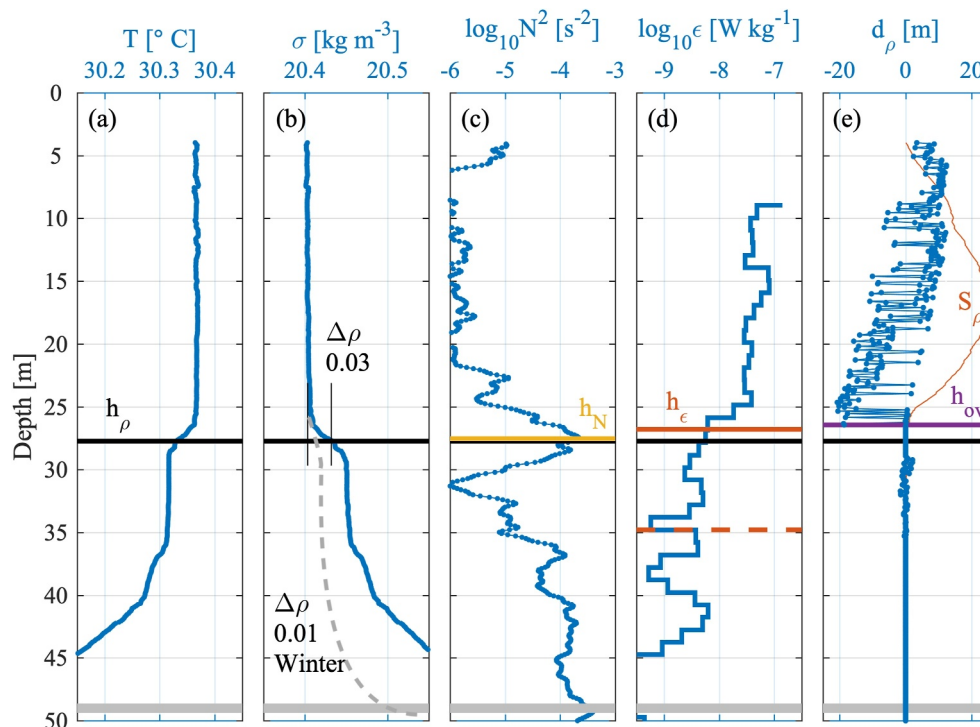


Figure 5. A typical profile of (a) temperature T , (b) density σ , (c) stratification N^2 and (d) dissipation rate ϵ and (e) Thorpe displacement d_ρ at 02:30 16-Jun 2017 (local time). The red line in (e) is the $0.03 \cdot S_\rho$. The black, yellow, magenta, purple and gray lines denote h_ρ , h_N , h_ϵ , h_{ov} , and H , respectively. The gray dotted line in (b) is a schematic profile to distinguish the density threshold between summer and winter.

temperature variations were large enough to cause strong stratification at the bottom of the DWL or DCL (i.e., a thin diurnal pycnocline following h_ρ and h_ϵ) even in winter. As a result, ϵ exhibited a similar pattern as N^2 due to the strong stratification inhibiting turbulence. In addition, another difference between the two cruises is that the remnant layer (the region between h_ρ and H) existed on summer nights but not on winter nights. In other words, the maximum depth of the DCL could not reach the seasonal mixed layer depth in summer, but it could expand quickly to the bottom of the seasonal mixed layer in winter.

3.3. Observed Depths in the ML

Although both h_ρ and h_ϵ have similar patterns of diurnal cycling, there are some details that deserve attention. Besides the h_ρ and h_ϵ , we also inspect two other observed depths that are calculated from stratification (h_N) and overturning zone (h_{ov}) as defined in Table 1. Figure 5 shows the typical profiles of T , σ , N^2 , ϵ , and d_ρ at 02:30 16-Jun 2017 (local time) to expound the definition of these 4 depths. We only focus on the summer cruise because it has a similar pattern in winter, but a difference is that we choose a smaller density threshold when calculating h_ρ in winter (density variation in winter is much more subtle, as shown by the gray dotted line in Figure 5b). The mixed layer depth calculated from the temperature profile is not shown because it is equal to h_ρ exactly for the temperature-dominated stratification. As for h_ϵ , it is the depth where ϵ decreases to an assumed background level ($10^{-9} \text{ W kg}^{-1}$) and no longer being influenced by surface forcing. The value of the background dissipation is chosen empirically based on the observed dissipation profiles and $10^{-9} \text{ W kg}^{-1}$ is a typical value in practice. In general, h_ϵ is the depth where the dissipation drops most rapidly but may defect due to the intermittency of turbulence. Therefore, manual rectifications are needed for some profiles. For example, h_ϵ marked by the red solid line is more reasonable than that marked by the dashed line in Figure 5d.

The time evolutions of the four depths are compared in Figure 6. In the nighttime, the dynamics was simple, and all depths coincided well with each other. Continuous cooling caused negative buoyancy flux at the sea surface inducing gravitational instability, resulting in overturning (h_{ov}) and homogeneous (h_ρ) regions. At the same time, convective turbulence induced by the gravitational instability enhanced the TKE dissipation rate, as evident in the

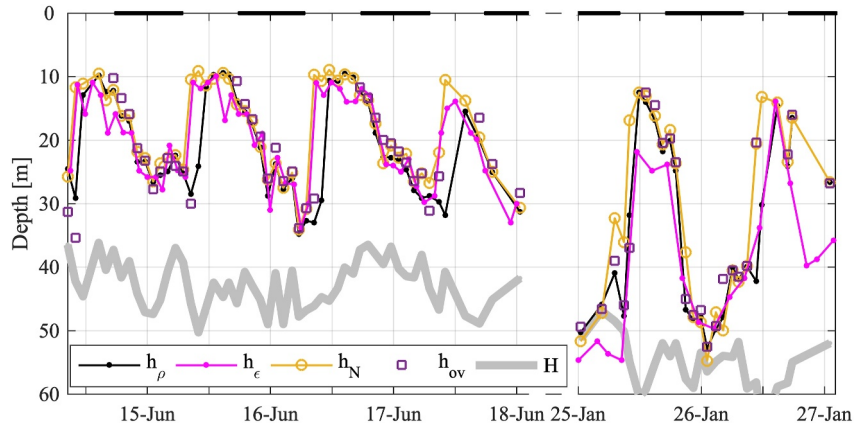


Figure 6. Time evolution of h_ρ , h_N , h_ϵ and h_{ov} .

DCL. In the daytime, by contrast, there were clear differences in the four depths. First, there were no distinct overturns detected during restratification, and h_{ov} (close to 0, not shown) failed to represent the depth of DWL as noted by Sutherland et al. (2014). Second, h_ρ had an ~ 2.5 hr delay in the early morning compared with h_ϵ and h_N . The stratification began to increase in the upper several meters when the heat (buoyancy) flux changed sign after the sunrise, resulting in the formation of the DWL and made h_N decrease quickly. At the same time, continuous heating and enhanced stratification weakened the convective turbulence so that the dissipation rate decreased immediately. However, the density change was smaller than the threshold (0.03 kg m^{-3}) at the base of the new DWL in the early morning, so that the calculated h_ρ could not recognize this shallower depth until the DWL got robust enough in the late morning. Lastly, h_ϵ is slightly larger than h_ρ or h_N , especially in the afternoon. Unlike at night, the source of turbulent kinetic energy during the day was related to wind mixing and the diurnal jet, which means momentum from wind is trapped in a thin near-surface layer (Hughes et al., 2020a; Hughes et al., 2020b). The shear turbulence was enhanced at the base of the shallow DWL, resulting in the larger h_ϵ during the daytime. Obviously, the evolutions of diurnal mixing/mixed depth are controlled by different dynamic processes during the daytime and nighttime, it is necessary to parameterize these depths separately.

3.4. Scaling the DWL Depth

Figure 7 shows the time evolutions of the observed depths (h_ϵ and h_ρ), diagnostic depths (D_T and D_p) and scaled depths (L_{MO} and L_Z) during the daytime of June 15 and 16. D_T and D_p are reasonable depths to represent the depth of DWL because they agreed well with h_ϵ in the morning and with h_ρ in the afternoon. L_{MO} greatly underestimates the DWL depth, while L_Z is well consistent with h_ϵ and h_ρ (or D_T and D_p) if multiplied by a constant. Therefore, L_Z is a suitable proxy for the mixed layer depth under stable stratification as previous studies demonstrated (Noh & Choi, 2018; Yoshikawa, 2015). Another advantage of L_Z is that only the wind and buoyancy flux are required to calculate this depth. As a result, we adopt the established scaling aL_Z to represent the depth of DWL in this study. Here, the constant a is estimated to be 1.2, for the observed depths (h_ϵ and h_ρ) is 1.2 times of L_Z .

3.5. Scaling the DCL Depth

Nighttime cooling drove the deepening of the DCL and the decrease of SST in the upper 30 m (Figure 8). In order to clarify the relationship among them, we adopt the Kraus-Turner type model (Dong & Kelly, 2004; Kraus & Turner, 1967; Qiu & Kelly, 1993):

$$\frac{\partial h_m}{\partial t} + \nabla \cdot \mathbf{U}_m = A_h \nabla^2 h_m + w_e, \quad (7)$$

$$\frac{\partial T_m}{\partial t} = \frac{Q_0 - q(-h_m)}{\rho_0 c_p h_m} - \mathbf{u}_m \cdot \nabla T_m + A_h \nabla^2 T - \frac{\Delta T w_e}{h_m}, \quad (8)$$

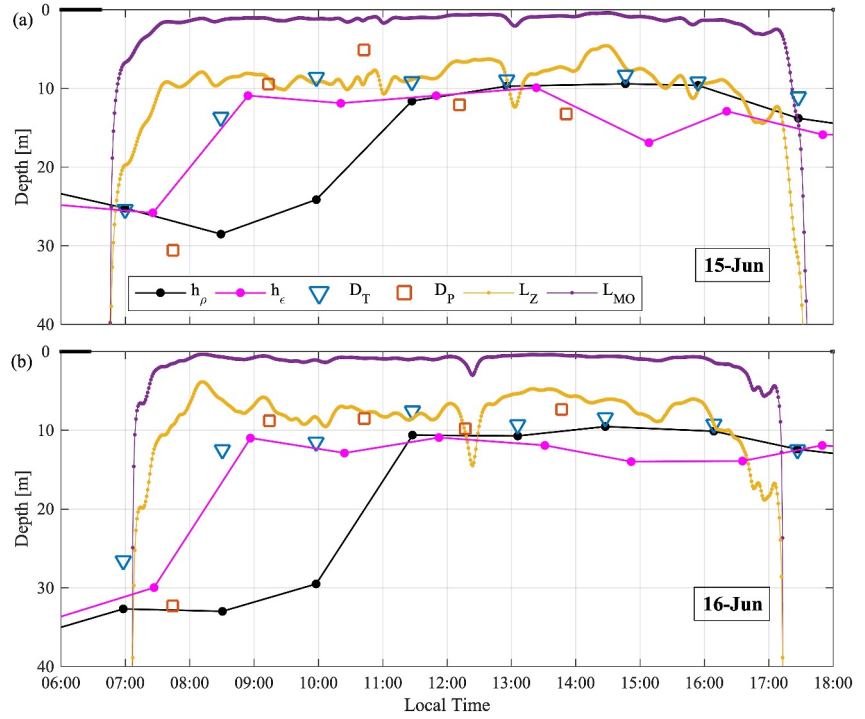


Figure 7. Time evolution of h_p , h_e , D_T , D_P , L_{MO} and L_Z during the daytime on 15-Jun and 16-Jun.

where h_m is the mixed layer depth and T_m is the mixed layer temperature (or bulk SST). \mathbf{u}_m and \mathbf{U}_m are the horizontal velocity and horizontal transport, respectively. A_h is the horizontal eddy diffusivity, ΔT is the temperature difference between the mixed layer and the layer just below the mixed layer, $\Delta T = \text{SST} - T_r$, where T_r is the reference temperature in the remnant layer. The entrainment velocity w_e is determined from the turbulent kinetic energy balance (Kraus & Turner, 1967),

$$\frac{1}{2}\alpha g h_m \nabla T w_e = m_0 u_*^3 + \frac{\alpha g}{\rho_0 c_p} \int_{-h_m}^0 q(z) dz - \frac{\alpha g h_m}{2\rho_0 c_p} (Q_0 + q(-h_m)) - m_c \frac{\alpha g h_m}{4\rho_0 c_p} (|Q_0| - Q_0), \quad (9)$$

where m_0 and m_c are constant coefficients. Following Davis et al. (1981) and Deardorff et al. (1969), we choose m_0 and m_c to be 0.5 and 0.83, respectively.

In the nighttime, the entrainment velocity w_e exhibited the same magnitude as the deepening rate of DCL (Figure 9a). The advection term ($-\mathbf{u}_m \cdot \nabla T_m$) and diffusion term ($A_h \nabla^2 T$) in temperature Equation 8 are relatively small and generally negligible (see Appendix A for the justification). As shown in Figure 9, the temperature tendency ($\partial T_m / \partial t$) can be balanced by the sum of heating ($\frac{Q_0 - q(-h_m)}{\rho_0 c_p h_m}$) and entrainment ($-\frac{\Delta T w_e}{h_m}$). The simplified equations are

$$\frac{\partial h_m}{\partial t} = w_e, \quad (10)$$

$$\frac{\partial T_m}{\partial t} = \frac{Q_0}{\rho_0 c_p h_m} - \frac{\Delta T w_e}{h_m}. \quad (11)$$

Combing the above two equations, one derives the equation of the DCL depth h_m

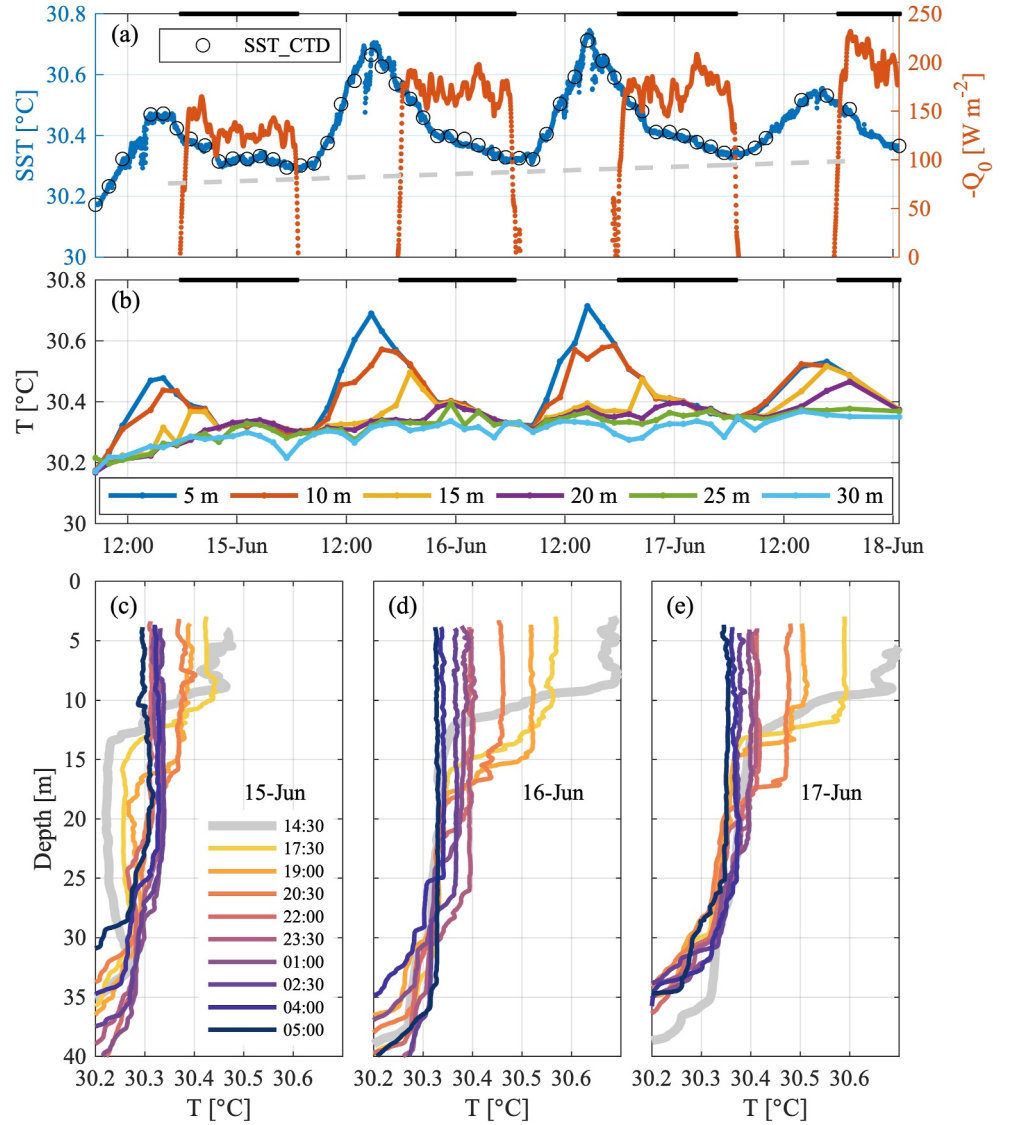


Figure 8. Time evolution of (a) underway SST, surface temperature from CTD profiles, net heat flux (b) temperature at different depths and temperature profiles at nighttime of (c) 15-Jun, (d) 16-Jun and (e) 17-Jun. Gray dashed line in (a) indicates the trend of the minimum SST at each night. (c)–(e) Share the same legend.

$$\frac{dh_m}{dt} + \frac{1}{\Delta T} \frac{dT_m}{dt} h_m = \frac{Q_0}{\rho_w c_p \Delta T} \cdot \frac{Q(t)}{Q(t)} \quad (12)$$

The general solution of Equation 12 is $h_m = (\int Q(t) e^{\int P(t) dt} dt + C) e^{-\int P(t) dt}$. When $t = t_0$ (Q_0 reverses sign and the ocean begins to lose heat), $C = h_0$, which is the initial depth formed in the late afternoon. Then, the deepening DCL can be expressed as a function of ΔT and Q_0 :

$$h_m(t) = \left(\int_{t_0}^t Q(t) e^{\int_0^t P(t) dt} dt + h_0 \right) e^{-\int_0^t P(t) dt} \quad (13)$$

To eliminate the dependence of the temperature profiles when determining ΔT , we chose the minimum SST at last night as T_r (see Appendix B for a discussion of this choice). As shown in Figure 10, the scaled h_m using both CTD

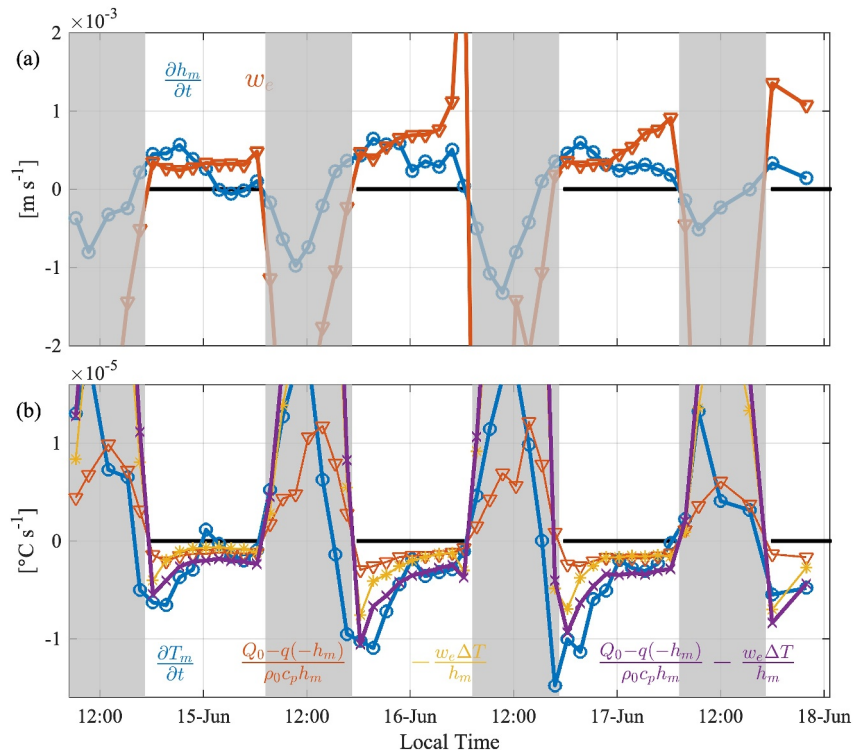


Figure 9. Time series of (a) deepening rate (blue) and entrainment velocity (red) in Equation 7. (b) SST tendency (blue), heating term (red), entrainment term (yellow) and the sum of heating and entrainment terms (purple) in Equation 8.

profiles and the underway data are well consistent with the observed mixing/mixed layer depths except the first night, which may have been affected by the rainfall a few days ago (the density ratio R_ρ was typically below 1). We also calculate h_{MS} according to Equation 1, where $N_{m}^2 = 1 \times 10^{-4} \text{ s}^{-2}$ is the average buoyancy frequency

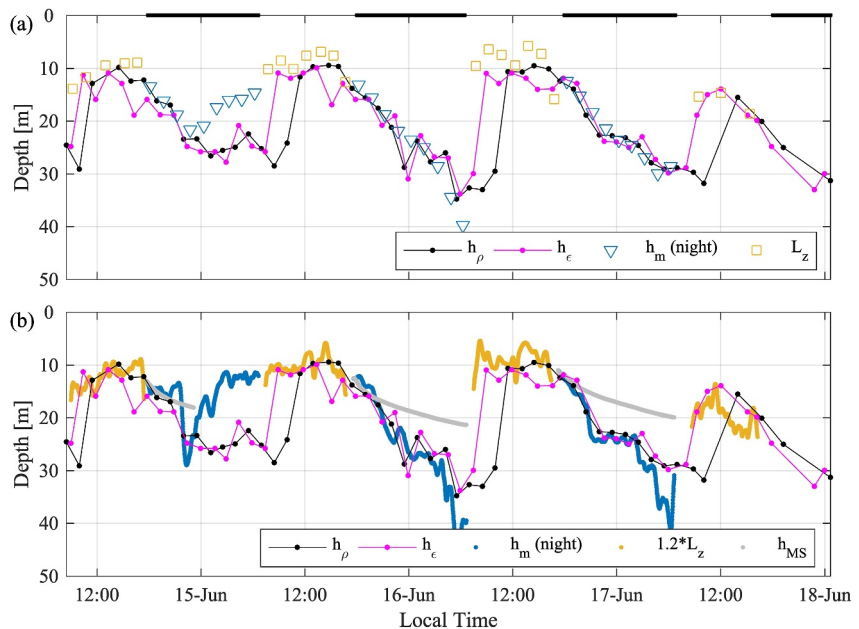


Figure 10. Comparison of observed MLD/XLD with scaled h_m , which the ΔT from (a) temperature profiles and (b) SST, respectively. Gray dot in (b) indicates the h_{MS} .

squared of the diurnal thermocline during the nighttime (Figure 4c). Here, the mixed layer depth in the late afternoon, that is h_0 , is used as the initial condition for h_{MS} . Evidently, h_{MS} underestimates the mixing/mixed layer depth in the nighttime (Figure 10b).

4. Summary

The diurnal cycling of the mixing/mixed layer depth in summer and winter was comparatively studied based on field observations during two cruises in the central South China Sea. Furthermore, we studied the response of diurnal mixing/mixed layer depth to the external forcing (wind and solar heating) and derived a functional relationship for the case when the stratification was dominated by the temperature and the horizontal transports were relatively small.

Although the diurnal cycling of turbulence and stratification was observed in both summer and winter, there were clear differences between them. In winter, the surface water obtained less solar shortwave radiation, and the stratification and warm layer were not as stable as summer. As a result, the nighttime convection could quickly destroy the relatively weak stratification and the diurnal convective layer quickly deepened to the bottom of the seasonal mixed layer. In summer, by contrast, the diurnal warm layer absorbed more heat during the daytime. The strong stratification limited the maximum depth of downward development of nighttime convection and the maximum depth of the diurnal convective layer could not reach the bottom of the seasonal mixed layer. In addition, the amplitude of diurnal SST variability in winter was not as strong as in summer and the stratification was controlled by both the salinity and temperature, not completely controlled by the temperature as in summer. These are the main reasons why the scaling Equation 13 derived from the temperature equation is not suitable for the winter cruise.

Considering the different external forcing and dynamics during the daytime and nighttime, we proposed a piecewise function to represent the response of the mixing/mixed layer depth to diurnal external forcing,

$$h_m(t) = \begin{cases} aL_z & ,(\text{daytime}) \\ \left(\int_{t_0}^t Q(t) e^{\int_{t_0}^t P(t) dt} dt + h_0 \right) e^{-\int_{t_0}^t P(t) dt} & ,(\text{nighttime}) \end{cases} \quad (14)$$

where $L_z = u_*^2 / (f\kappa B_0)^{1/2}$, $P(t) = \frac{1}{\Delta T} \frac{dT_m}{dt} = \frac{d}{dt} \ln(\Delta T)$ and $Q(t) = \frac{Q_0}{\rho_0 c_p \Delta T}$, the constant $a = 1.2$, h_0 is the stable warm layer depth in the late afternoon. Strictly speaking, the scaled h_m here is the proxy of mixing layer depth (h_e) as shown in Figure 10b. Considering the dynamic relationship between mixing and mixed layer depth, we can use Equation 14 to represent both.

5. Discussion

The diurnal cycle of the mixed layer was essentially the alternation of the diurnal warm layer and convective layer, which was mainly driven by daytime warming and nighttime cooling, respectively. Under stable stratification conditions in the daytime, the wind-induced shear contributed to turbulence generation in the diurnal warm layer and the thickness of this layer could well be scaled by L_z following previous studies (Noh & Choi, 2018; Yoshikawa, 2015). In the nighttime, the deepening of a mixed layer based on the afternoon warm layer (h_0) could be derived from the simplified one-dimensional heat balance. From the simplified temperature Equation 11, there are two processes accounting for the evolution of the accumulated heat in surface seawater. On the one hand, the surface water loses heat leading to a decrease in the SST (heating term). On the other hand, the overturning entrains the colder water in the remnant layer just below and induces downward heat fluxes (entrainment term). Compared with Equation 11, Equation 1 further ignores the entrainment term when the buoyancy flux is dominated by heat flux. In fact, the heating and entrainment terms had equal contributions to temperature tendency (Figure 9b), which is why Equation 1 underestimates the diurnal convective layer depth (Figure 10b). Through Equation 14, we can estimate the diurnal mixing/mixed layer depth by time-dependent (bulk) SST, surface net heat flux, and wind stress, which are easier to obtain than the CTD or dissipation profiles. However, it is only available when the density stratification is dominated by the temperature since Equation 14 is derived from the temperature equation. For example, the stratification was dominated by the salinity on June 15, so that the

estimated h_m is inconsistent with the observed h_p and h_e on the first night (Figure 10). Besides, it will not work either when the horizontal transport is significant as the simplified equation ignores the advection term.

Under moderate (or weak) wind and clear days in the tropical open ocean, daytime heating and nighttime cooling are the dominant factors in controlling the mixing/mixed layer depth. However, the surface mixed layer is also affected by other processes, such as rainfall events, Langmuir circulation, frontal process, and so on. To better understand the diurnal evolution of the surface mixed layer, more targeted observations (which can resolve more dynamic processes) should be investigated, as well as high-resolution numerical simulations.

Appendix A: Assessment of the Contribution of Advection

We evaluated the contribution of the advection term ($-\mathbf{u}_m \cdot \nabla T_m$) in the temperature Equation 8 through the two orthogonal transects after completing the time series observations. Figure A1 shows the temperature and velocity sections, as well as the average value of the upper 30 m. The magnitude of the advection term is about $1 \times 10^{-6} \text{C/s}$, which is close to the result based on CMEMS (Copernicus-Marine Environment Monitoring Service) reanalysis data (not shown). Compared with other dominant terms (Figure 9b), the contribution of advection terms is relatively small and can be ignored. The diffusion term ($A_h \nabla^2 T$) is much smaller and not considered.

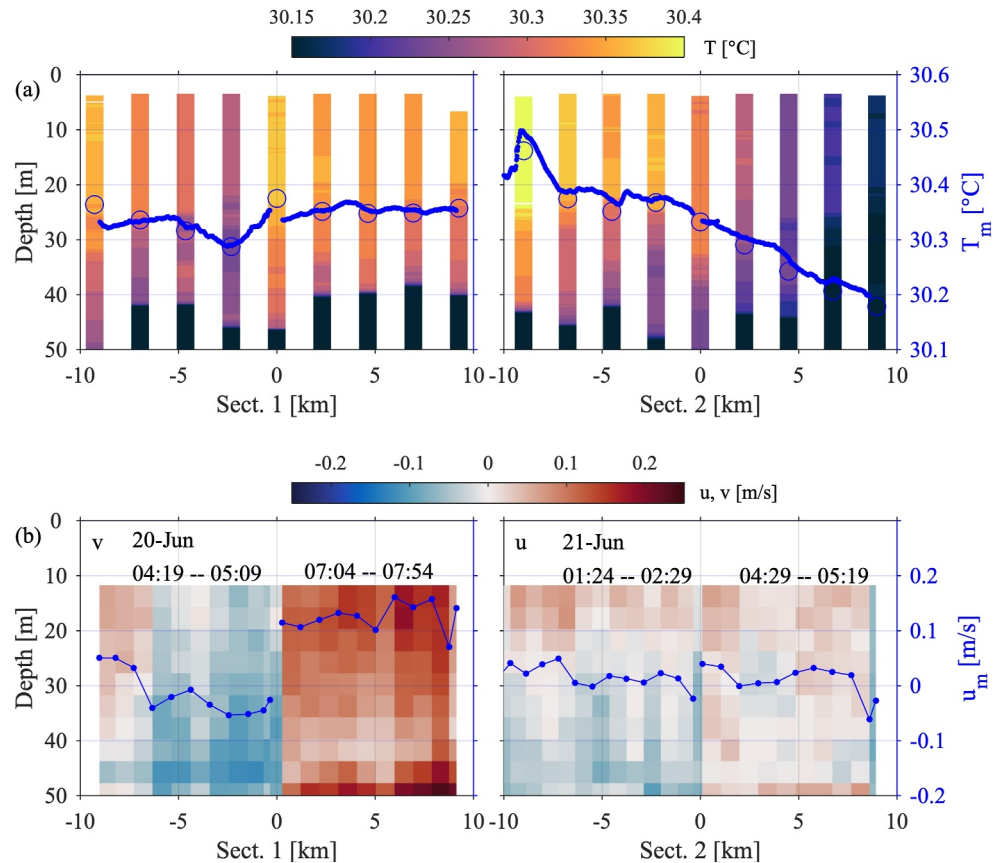


Figure A1. Transects of (a) temperature and (b) velocity. The blue cycle and dot-line indicate the upper 30 m averaged temperature T_m and velocity u_m , respectively. Blue dot in (a) indicate the underway SST. Refer to Figure 1 for the location of transects.

Appendix B: Determination of the Reference Temperature

The reference temperature T_r is the key factor to determine ΔT , which is the dominant factor in Equation 14. As a result, the parameterized h_m is sensitive to T_r . As shown in Figure B1, we have carried out several sensitivity tests on reference temperature. Strictly speaking, T_r is the temperature in the remnant layer. However, T_r can be approximated from SST if we do not have the temperature profile. In ideal conditions (ignore the advection effect), the remnant layer comes from the DCL before the shallow DWL cap exists at the surface. As a result, T_r can be represented as the minimum SST just before the last sunrise. Considering that the lowest SST had a trend of $0.03^\circ\text{C}/\text{day}$ in three nights (gray dashed line in Figure 8a), we chose $T_r = \min(\text{SST}) - 0.03$ (the minimum SST of the previous night) as the reference temperature in this study.

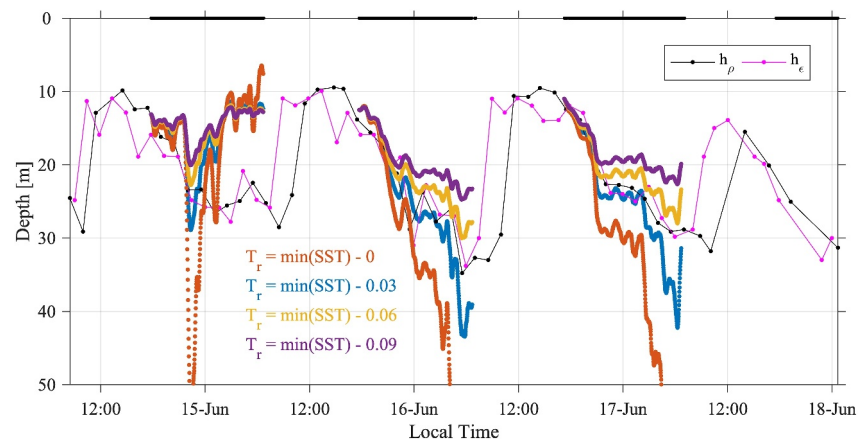


Figure B1. Calculated h_m with different reference temperature T_r .

Data Availability Statement

The in situ data analyzed in this study are available on the Science Data Bank (Cao & Liu, 2024, <https://doi.org/10.57760/sciencedb.07827>).

References

- Belcher, S. E., Grant, A. L. M., Hanley, K. E., Fox-Kemper, B., Van Roekel, L., Sullivan, P. P., et al. (2012). A global perspective on Langmuir turbulence in the ocean surface boundary layer. *Geophysical Research Letters*, 39(18). <https://doi.org/10.1029/2012GL052932>
- Brainerd, K. E., & Gregg, M. C. (1993). Diurnal restratification and turbulence in the oceanic surface mixed layer: 1. Observations. *Journal of Geophysical Research*, 98(C12), 22645–22656. <https://doi.org/10.1029/93JC02297>
- Brainerd, K. E., & Gregg, M. C. (1995). Surface mixed and mixing layer depths. *Deep-Sea Research I*, 42(9), 1521–1543. [https://doi.org/10.1016/0967-0637\(95\)00068-H](https://doi.org/10.1016/0967-0637(95)00068-H)
- Cao, Z., & Liu, Z. (2024). Experimental dataset for 'scaling the diurnal mixing/mixed layer depth in the tropical ocean: A case study in the South China sea'. [Dataset]. <https://doi.org/10.57760/sciencedb.07827>. *Science Data Bank*.
- Chu, P. C., & Fan, C. (2010). Optimal linear fitting for objective determination of ocean mixed layer depth from glider profiles. *Journal of Atmospheric and Oceanic Technology*, 27(11), 1893–1898. <https://doi.org/10.1175/2010jtecho804.1>
- D'Asaro, E. A. (2014). Turbulence in the upper-ocean mixed layer. *Annual Review of Marine Science*, 6, 101–115. <https://doi.org/10.1146/annurev-marine-010213-135138>
- Davis, R., DeSzoeke, R., & Niiler, P. (1981). Variability in the upper ocean during MILE. Part II: Modeling the mixed layer response. *Deep-Sea Research, Part A: Oceanographic Research Papers*, 28(12), 1453–1475. [https://doi.org/10.1016/0198-0149\(81\)90092-3](https://doi.org/10.1016/0198-0149(81)90092-3)
- Deardorff, J. W., Willis, G. E., & Lilly, D. K. (1969). Laboratory investigation of non-steady penetrative convection. *Journal of Fluid Mechanics*, 35(1), 7–31. <https://doi.org/10.1017/S0022112069000942>
- de Boyer Montégut, C., Madec, G., Fischer, A. S., Lazar, A., & Iudicone, D. (2004). Mixed layer depth over the global ocean: An examination of profile data and a profile-based climatology. *Journal of Geophysical Research*, 109(C12). <https://doi.org/10.1029/2004jc002378>
- Dong, S., & Kelly, K. A. (2004). Heat budget in the gulf stream region: The importance of heat storage and advection. *Journal of Physical Oceanography*, 34(5), 1214–1231. [https://doi.org/10.1175/1520-0485\(2004\)034<1214:Hbits>2.0.Co;2](https://doi.org/10.1175/1520-0485(2004)034<1214:Hbits>2.0.Co;2)
- Fairall, C. W., Bradley, E. F., Hare, J. E., Grachev, A. A., & Edson, J. B. (2003). Bulk parameterization of air-sea fluxes: Updates and verification for the COARE algorithm. *Journal of Climate*, 16(4), 571–591. [https://doi.org/10.1175/1520-0442\(2003\)016<0571:bpoasf>2.0.co;2](https://doi.org/10.1175/1520-0442(2003)016<0571:bpoasf>2.0.co;2)
- Franks, P. J. (2014). Has sverdrup's critical depth hypothesis been tested? Mixed layers vs. turbulent layers. *ICES Journal of Marine Science*, 72(6), 1897–1907. <https://doi.org/10.1093/icesjms/fsu175>
- Giunta, V., & Ward, B. (2022). Ocean mixed layer depth from dissipation. *Journal of Geophysical Research: Oceans*, 127(4), e2021JC017904. <https://doi.org/10.1029/2021JC017904>

Acknowledgments

We thank the crew of the R/V TAN KAH KEE (TKK) for their assistance in data collection. This work was jointly supported by the Natural Science Foundation of Fujian Province of China (2021J02005), the National Key R&D Program of China (2023YFE0126700 and 2022YFA1003804), and the National Natural Science Foundation of China (92258301). DW's participation of this work was supported by the National Natural Science Foundation of China (42006010) and the Fundamental Research Funds for the Central Universities of Xiamen University (20720240103). We thank the two anonymous reviewers for their constructive suggestions and comments.

- Goh, G., & Noh, Y. (2013). Influence of the Coriolis force on the formation of a seasonal thermocline. *Ocean Dynamics*, 63(9–10), 1083–1092. <https://doi.org/10.1007/s10236-013-0645-x>
- Holte, J., & Talley, L. (2009). A new algorithm for finding mixed layer depths with applications to argo data and subantarctic mode water formation. *Journal of Atmospheric and Oceanic Technology*, 26(9), 1920–1939. <https://doi.org/10.1175/2009jtecho543.1>
- Huang, C., Wang, W., & Huang, R. (2007). Climate variability in the equatorial Pacific ocean induced by decadal variability of mixing coefficient. *Journal of Physical Oceanography*, 37(5), 1163–1176. <https://doi.org/10.1175/jpo3060.1>
- Huang, P., Lu, Y., & Zhou, S. (2018). An objective method for determining ocean mixed layer depth with applications to WOCE data. *Journal of Atmospheric and Oceanic Technology*, 35(3), 441–458. <https://doi.org/10.1175/jtech-d-17-0104.1>
- Hughes, K. G., Moun, J. N., & Shroyer, E. L. (2020a). Evolution of the velocity structure in the diurnal warm layer. *Journal of Physical Oceanography*, 50(3), 615–631. <https://doi.org/10.1175/jpo-d-19-0207.1>
- Hughes, K. G., Moun, J. N., & Shroyer, E. L. (2020b). Heat transport through diurnal warm layers. *Journal of Physical Oceanography*, 50(10), 2885–2905. <https://doi.org/10.1175/jpo-d-20-0079.1>
- Jalali, M., Chalamalla, V. K., & Sarkar, S. (2017). On the accuracy of overturn-based estimates of turbulent dissipation at rough topography. *Journal of Physical Oceanography*, 47(3), 513–532. <https://doi.org/10.1175/JPO-D-15-0169.1>
- Kara, A. B., Rochford, P. A., & Hurlburt, H. E. (2000). An optimal definition for ocean mixed layer depth. *Journal of Geophysical Research*, 105(C7), 16803–16821. <https://doi.org/10.1029/2000jc900072>
- Kawai, Y., & Wada, A. (2007). Diurnal Sea surface temperature variation and its impact on the atmosphere and ocean: A review. *Journal of Oceanography*, 63(5), 721–744. <https://doi.org/10.1007/s10872-007-0063-0>
- Kraus, E. B., & Turner, J. S. (1967). A one-dimensional model of the seasonal thermocline II. The general theory and its consequences. *Tellus*, 19(1), 98–106. <https://doi.org/10.3402/tellusa.v19i1.9753>
- Lombardo, C. P., & Gregg, M. C. (1989). Similarity scaling of viscous and thermal dissipation in a convecting surface boundary layer. *Journal of Geophysical Research*, 94(C5), 6273–6284. <https://doi.org/10.1029/jc094ic05p06273>
- Lozovatsky, I., Figueroa, M., Roget, E., Fernando, H. J. S., & Shapovalov, S. (2005). Observations and scaling of the upper mixed layer in the North Atlantic. *Journal of Geophysical Research*, 110(C5). <https://doi.org/10.1029/2004JC002708>
- Lukas, R., & Lindstrom, E. (1991). The mixed layer of the western equatorial Pacific Ocean. *Journal of Geophysical Research*, 96(S01), 3343–3357. <https://doi.org/10.1029/90jc01951>
- Marshall, J., & Schott, F. (1999). Open-ocean convection: Observations, theory, and models. *Reviews of Geophysics*, 37(1), 1–64. <https://doi.org/10.1029/98RG02739>
- Noh, Y., & Choi, Y. (2018). Comments on “Langmuir turbulence and surface heating in the ocean surface boundary layer”. *Journal of Physical Oceanography*, 48(2), 455–458. <https://doi.org/10.1175/jpo-d-17-0135.1>
- Ohlmann, J. C., & Siegel, D. A. (2000). Ocean radiant heating. Part II: Parameterizing solar radiation transmission through the upper ocean. *Journal of Physical Oceanography*, 30(8), 1849–1865. [https://doi.org/10.1175/1520-0485\(2000\)030<1849:orhpi>2.0.co;2](https://doi.org/10.1175/1520-0485(2000)030<1849:orhpi>2.0.co;2)
- Paulson, C. A., & Simpson, J. J. (1977). Irradiance measurements in the upper ocean. *Journal of Physical Oceanography*, 7(6), 952–956. [https://doi.org/10.1175/1520-0485\(1977\)007<0952:Imituo>2.0.Co;2](https://doi.org/10.1175/1520-0485(1977)007<0952:Imituo>2.0.Co;2)
- Price, J. F., Weller, R. A., & Pinkel, R. (1986). Diurnal cycling: Observations and models of the upper ocean response to diurnal heating, cooling and wind mixing. *Journal of Geophysical Research*, 91(C7), 8411–8427. <https://doi.org/10.1029/jc091ic07p08411>
- Qiu, B., & Kelly, K. A. (1993). Upper-Ocean heat balance in the kuroshio extension region. *Journal of Physical Oceanography*, 23(9), 2027–2041. [https://doi.org/10.1175/1520-0485\(1993\)023<2027:uohbit>2.0.co;2](https://doi.org/10.1175/1520-0485(1993)023<2027:uohbit>2.0.co;2)
- Roget, E., Lozovatsky, I., Sanchez, X., & Figueroa, M. (2006). Microstructure measurements in natural waters: Methodology and applications. *Progress in Oceanography*, 70(2–4), 126–148. <https://doi.org/10.1016/j.pocean.2006.07.003>
- Shay, T. J., & Gregg, M. C. (1984). Turbulence in an oceanic convective mixed layer. *Nature*, 310(5975), 282–285. <https://doi.org/10.1038/310282a0>
- Soloviev, A., & Lukas, R. (1997). Observation of large diurnal warming events in the near-surface layer of the western equatorial Pacific warm pool. *Deep-Sea Research, Part A: Oceanographic Research Papers*, 44(6), 1055–1076. [https://doi.org/10.1016/S0967-0637\(96\)00124-0](https://doi.org/10.1016/S0967-0637(96)00124-0)
- Somavilla, R., Gonzalez-Pola, C., & Fernandez-Diaz, J. (2017). The warmer the ocean surface, the shallower the mixed layer. How much of this is true? *Journal of Geophysical Research: Oceans*, 122(9), 7698–7716. <https://doi.org/10.1002/2017JC013125>
- Sutherland, G., Reverdin, G., Marié, L., & Ward, B. (2014). Mixed and mixing layer depths in the ocean surface boundary layer under conditions of diurnal stratification. *Geophysical Research Letters*, 41(23), 8469–8476. <https://doi.org/10.1002/2014GL061939>
- Thomson, R. E., & Fine, I. V. (2003). Estimating mixed layer depth from oceanic profile data. *Journal of Atmospheric and Oceanic Technology*, 20(2), 319–329. [https://doi.org/10.1175/1520-0426\(2003\)020<0319:EMLDFO>2.0.CO;2](https://doi.org/10.1175/1520-0426(2003)020<0319:EMLDFO>2.0.CO;2)
- Ushijima, Y., & Yoshikawa, Y. (2019). Mixed layer depth and sea surface warming under diurnally cycling surface heat flux in the heating season. *Journal of Physical Oceanography*, 49(7), 1769–1787. <https://doi.org/10.1175/jpo-d-18-0230.1>
- Wolk, F., Yamazaki, H., Seuront, L., & Lueck, R. G. (2002). A new free-fall profiler for measuring biophysical microstructure. *Journal of Atmospheric and Oceanic Technology*, 19(5), 780–793. [https://doi.org/10.1175/1520-0426\(2002\)019<0780:anfpp>2.0.co;2](https://doi.org/10.1175/1520-0426(2002)019<0780:anfpp>2.0.co;2)
- Yoshikawa, Y. (2015). Scaling surface mixing/mixed layer depth under stabilizing buoyancy flux. *Journal of Physical Oceanography*, 45(1), 247–258. <https://doi.org/10.1175/jpo-d-13-0190.1>
- Zheng, R., & Jing, Z. (2024). Diurnal variability of mixed layer overturning instabilities from glider array observations in the South China sea. *Geophysical Research Letters*, 51(11), e2023GL107694. <https://doi.org/10.1029/2023GL107694>
- Zilitinkevich, S. (1972). On the determination of the height of the Ekman boundary layer. *Boundary-Layer Meteorology*, 3(2), 141–145. <https://doi.org/10.1007/BF02033914>